Opto-Electronic
Advances

ISSN 2096-4579 CN 51-1781/TN

A highly sensitive LITES sensor based on a multi-pass cell with dense spot pattern and a novel quartz tuning fork with low frequency

Yahui Liu, Shunda Qiao, Chao Fang, Ying He, Haiyue Sun, Jian Liu and Yufei Ma

Citation: Liu YH, Qiao SD, Fang C, et al. A highly sensitive LITES sensor based on a multi-pass cell with dense spot pattern and a novel quartz tuning fork with low frequency. *Opto-Electron Adv* **7**, 230230(2024).

https://doi.org/10.29026/oea.2024.230230

Received: 20 December 2023; Accepted: 26 January 2024; Published online: 18 February 2024

Opto-Electronic Advances

Article
March 2024, Vol. 7, No. 3

DOI: 10.29026/oea.2024.230230

A highly sensitive LITES sensor based on a multi-pass cell with dense spot pattern and a novel quartz tuning fork with low frequency

Yahui Liu[1,2], Shunda Qiao[1,2], Chao Fang[1,2], Ying He[1,2], Haiyue Sun[1,2], Jian Liu[3] and Yufei Ma[1,2]*

A highly sensitive light-induced thermoelectric spectroscopy (LITES) sensor based on a multi-pass cell (MPC) with dense spot pattern and a novel quartz tuning fork (QTF) with low resonance frequency is reported in this manuscript. An erbium-doped fiber amplifier (EDFA) was employed to amplify the output optical power so that the signal level was further enhanced. The optical path length (OPL) and the ratio of optical path length to volume (RLV) of the MPC is 37.7 m and 13.8 cm^{-2}, respectively. A commercial QTF and a self-designed trapezoidal-tip QTF with low frequency of 9461.83 Hz were used as the detectors of the sensor, respectively. The target gas selected to test the performance of the system was acetylene (C_2H_2). When the optical power was constant at 1000 mW, the minimum detection limit (MDL) of the C_2H_2-LITES sensor can be achieved 48.3 ppb when using the commercial QTF and 24.6 ppb when using the trapezoidal-tip QTF. An improvement of the detection performance by a factor of 1.96 was achieved after replacing the commercial QTF with the trapezoidal-tip QTF.

Keywords: light-induced thermoelectric spectroscopy; quartz tuning fork; multi-pass cell; gas sensing

Liu YH, Qiao SD, Fang C et al. A highly sensitive LITES sensor based on a multi-pass cell with dense spot pattern and a novel quartz tuning fork with low frequency. *Opto-Electron Adv* **7**, 230230 (2024).

Introduction

Gas sensing technology is playing an important role in human production and activities[1–11], and the gas sensor based on laser absorption spectroscopy (LAS) is one of the mainstream types. It offers some unique advantages such as high selectivity, high sensitivity and rapid responsiveness[12–21]. According to the different detective modes, the LAS can be segmented into three types: 1) the direct detection technology including tunable diode laser absorption spectroscopy (TDLAS)[22]; 2) the cavity enhanced absorption spectroscopy (CEAS)[23–25]; 3) and the indirect detection technology whose typical representations are photoacoustic spectroscopy (PAS) and quartz enhanced photoacoustic spectroscopy (QEPAS)[26–29]. Among these technologies, PAS inverts the gas concentration by detecting the acoustic signal generated after the laser is absorbed by the gas, and thus it can achieve the no background detection[30,31]. QEPAS replaces the traditional microphone with quartz tuning fork (QTF) as a detection element, which can effectively filter the 1/*f* noise of the system[32].

[1]National Key Laboratory of Science and Technology on Tunable Laser, Harbin Institute of Technology, Harbin 150000 China; [2]Zhengzhou Research Institute, Harbin Institute of Technology, Zhengzhou 450000, China; [3]Advanced Microscopy and Instrumentation Research Center, School of Instrumentation Science and Engineering, Harbin Institute of Technology, Harbin 150080, China.

*Correspondence: YF Ma, E-mail: mayufei@hit.edu.cn

Received: 20 December 2023; Accepted: 26 January 2024; Published online: 18 February 2024

Although QEPAS offers an outstanding performance for gas sensing, there are some shortcomings prevent it from being used in some special application scenarios. For example, since QTF generates an effective signal only when placed in an environment filled with the test gas, QEPAS is powerless to detect the corrosive and acid gases such as hydrogen fluoride (HF), hydrogen sulfide (H_2S) and hydrogen chloride (HCl)[33–35]. In order to improve the disadvantages of QEPAS, Ma et al. reported a different detection technology named light-induced thermoelectric spectroscopy (LITES) in 2018[36]. The detection segment of this method is still QTF, but the signal generation no longer relies on acoustic wave. When the modulated laser is absorbed by the test gas in a gas chamber, the transmitted laser will carry the concentration information of the gas. After absorbing the energy of this part of the laser, the QTF will perform a signal conversion process from light to heat and then to electricity. By demodulating the electrical signal, the concentration information of the gas can be obtained[37–39]. In LITES based gas sensors, the QTF needn't be surrounded with the test gas, which makes it possible to achieve non-invasive detection[40–42]. In addition, since LITES relies on the thermoelastic deformation generated by the absorption of laser energy to generate current signals, it has an extremely wide response bandwidth compared to traditional photodetectors and is expected to become a means of detecting gases in the full-band spectrum[43,44].

Based on the principle of Beer-Lambert's law, the strength of the absorbed signal in a gas sensing system is proportional to the gas absorption length[45]. Multi-pass cells (MPCs) are usually adopted to increase the absorption length and therefore regarded as a key device to improve the detection performance of LITES system[46,47]. Herriott cell is the most widely used MPC because of its simple structure and high stability. In 2019, He et al. firstly reported a LITES sensing system combined with a Herriott cell with an effective absorption length of 10.1 m[48]. Recently, MPCs with dense spot patterns are gradually being used as a new gas absorption device[49–53]. MPCs with dense spot patterns have a large ratio of optical path length to volume (RLV) which makes it potentially a key element for integrated ultra-highly sensitive LITES based sensors.

Another vital component in LITES system is QTF[54–56]. Currently, the standard commercial QTFs with a resonant frequency of ~32.76 kHz are most commonly used. In order to match the resonance frequency, the system also need a high modulation frequency. In a very short modulation period, the QTF can only absorb a very limited amount of laser energy, and thus converts a weak piezoelectric signal. Using a low-frequency QTF as a detector provides a longer energy accumulation time, which will effectively improve the detection performance of the LITES system.

In this manuscript, a highly sensitive LITES sensor based on a MPC with dense spot pattern and a novel QTF with low frequency is reported for the first time. The MPC has an optical path length (OPL) of 37.7 m, a volume of 272 mL, and forms a spot distribution pattern with 4 concentric rings on the mirrors to enhance laser absorption. Besides, a self-designed trapezoidal-tip QTF with low-frequency of 9461.83 Hz was used to further enhance the sensing performance. Acetylene (C_2H_2) was selected as the target gas for testing to evaluate the sensor performance.

Experimental setup

Design of multi-pass cell

The White cell and the Herriott cell are the two most typical MPCs and have a long history of application in gas sensing[57–59]. Especially the Herriott cell has many advantages such as simple structure, stable optical path, and easy adjustment, which makes it almost has been the unquestionable choice in gas sensors. However, it also has some drawbacks that limit further improvements in sensor performance. The spots distribution of it is usually individually circular or elliptical, which makes its mirror utilization extremely low. Furthermore, when the number of reflections increases, spots with adjacent positions tend to overlap and it will introduce interference noise into the system. MPC with dense spot patterns is an improve design of the Herriott cell, which not only retains the previous features, but significantly improves the mirror utilization[60,61].

In order to obtain the parameters of MPC, a computational model based on vector reflection theory was designed. It is capable of tracing beam transmitted by reflection between two identical spherical mirrors placed co-axially. The key parameters in the MPC, including incident position, incident angle, diameter of the mirror, radius of curvature and distance between the two mirrors, are varied to obtain different spot distribution effects. There are several requirements that can be used as criteria for parameter selection: 1) In multiple reflections, the beam does not overflow from the edge of the mirrors unless it is emitted from the set perforation position; 2) Having a regular and non-overlapping spot distribution pattern to facilitate optical path length adjustment and avoid interference noise; 3) Achieving as many reflections as possible with a short base length; 4) The outgoing beam exits the outlet completely with good beam quality.

For convenience, the design of MPC was based on regular-sized mirrors with a diameter of 2 inches and a radius of curvature of 100 mm. In order to simulate the spots shape on the mirror, several parallel straight lines were used to construct the beam model, and the diameter of the beam was set to 600 μm. The parameter settings of MPC are shown in Fig. 1(a). The perforation diameter on the mirrors was set to 2 mm to allow for incident and outgoing beams. Based on the established computational model, when the distance of the mirrors, the incident angles θ and Φ were set to 137.78 mm, −7.23° and −5.43°, respectively, and the incident position coordinate was set to 20.18 mm and 3.42 mm, the spot distribution with four concentric circles was obtained. The simulation on the incident mirror is shown in Fig. 1(b). The beam was reflected 274 times and then exits through the exit perforation located on the other side. The volume of the MPCs was considered to be the cylindrical-like region between the two spherical mirrors, which is approximately equal to the volume of sample gas that the gas chamber can hold. The volume of this MPC is 272.6 mL and the OPL is 37.7 m, which gives a RLV of 13.8 cm^{-2}. Compared to a commercial Herriott cell (HC10L-M02, Thorlabs) whose RLV is about 1.49 cm^{-2}, there was a ~8-fold improvement. The plano-concave spherical mirrors with through-holes were processed based on the acquired parameters and subsequently coated with silver to achieve a high reflectivity across a broad range of wavelengths. It can provide greater than 95% reflectivity in the wavelength range of 400–12000 nm. The spot distribution obtained using a He-Ne laser is shown in Fig. 1(c). Although the quality of the beam is degraded due to multiple reflections and some of the spots become unclear, the shape of the actual spot still matched well with the simulation.

The self-designed QTF

The QTFs used in this manuscript are shown in Fig. 2(a), and QTF1 and QTF2 represents the commercial QTF and the self-designed trapezoidal-tip QTF, respectively. Compared to the standard commercial QTF, the self-designed QTF has an optimized dimension. A 3D model of the QTF was built based on COMSOL software, and finite element analysis was used to optimize the parameters such as the width and length of the fork fingers as well as the thickness in order to obtain a lower resonance frequency, the highest average charge density and maximum surface stress. In addition, it has a unique trapezoidal tip that enables it to generate a larger piezoelectric signal at resonance, which is because the trapezoidal-tip improves the stress distribution in the fork fingers and facilitates an increase in the Coriolis force and charge generation rate. The resonant frequencies of two QTFs were measured, and the normalized data was fitted using the Lorentz function, as shown in Fig. 2(b). The resonance frequencies (f) of the commercial QTF and the trapezoidal-tip QTF are 32.753 kHz and 9641.83 Hz, with response bandwidths of Δf_1 = 3.12

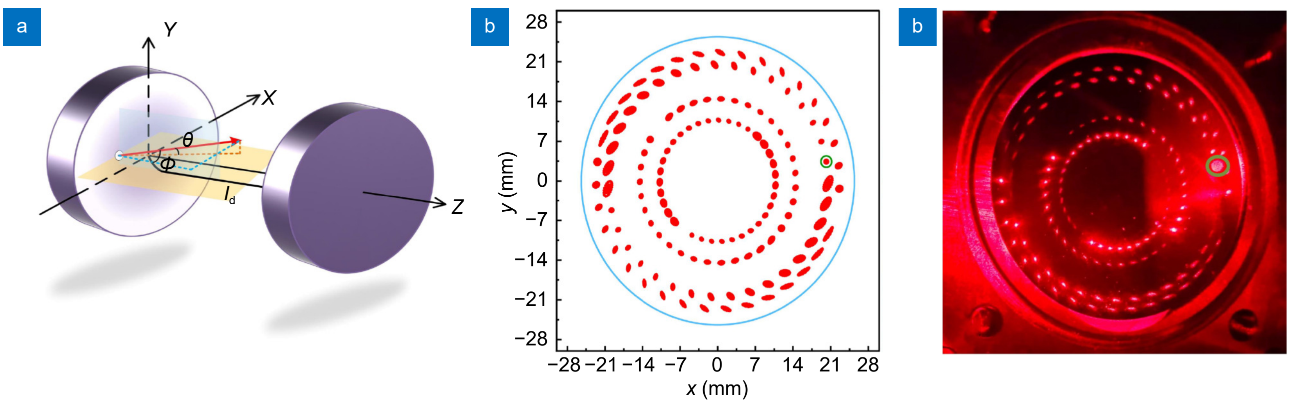

Fig. 1 | Structure parameter diagram of MPC and spot distribution on the surface of the incident mirror, where the green circle represents the location of the incident perforation. (**a**) Structure parameter diagram of MPC. (**b**) Simulation based on the established computational model. (**c**) Spot distribution obtained with a He-Ne laser.

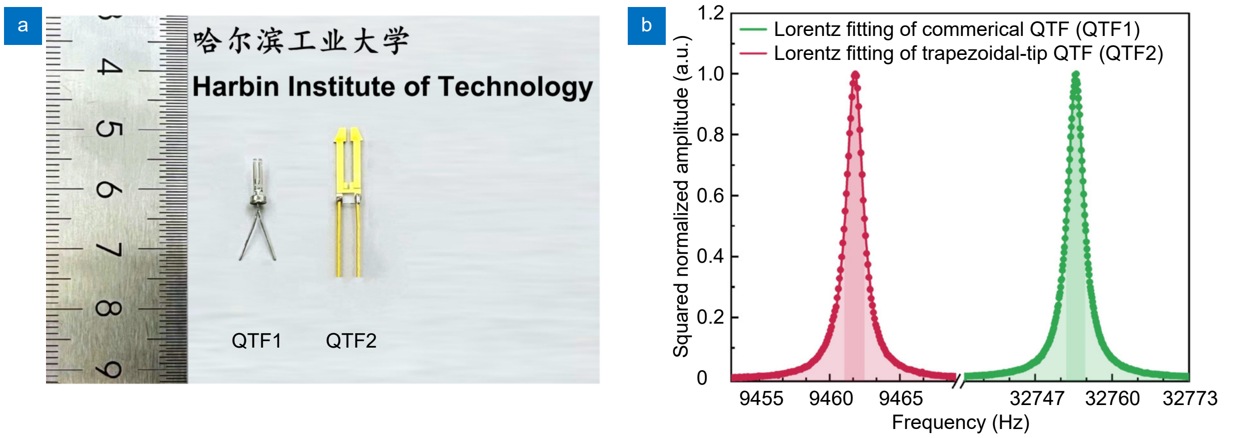

Fig. 2 | The features of two QTFs. (**a**) A photograph of the QTFs. (**b**) Frequency response of the commercial QTF (line in green) and the trapezoidal-tip QTF (line in red).

Hz and Δf_2 = 1.47 Hz, respectively. And the related quality factors (calculated with the formula $Q=f/\Delta f$) are 10565 and 6559, respectively. Compared to commercial QTF, the trapezoidal-tip QTF has a ~70% decrease in frequency and is beneficial to increase the energy accumulation time[62]. In addition, instead of using silver-plated electrodes as in commercial QTFs, the trapezoidal-tip QTF uses gold-plated electrodes to reduce resistance.

Sensor configuration

The schematic of the C_2H_2-LITES sensor based on a multi-pass cell with dense spot pattern is shown in Fig. 3. A strong absorption line of C_2H_2 located at 1530.37 nm (6534.37 cm^{-1}) was selected to verify the detection performance. The system was equipped with a continuous wave (CW), distributed feedback (DFB) diode laser as the laser excitation source, and the output power was amplified by an erbium-doped fiber amplifier (EDFA). The operating temperature and center current of the laser were set to 29°C and 92 mA, respectively, and the output power of the EDFA was in the range of 300 mW to 1000 mW. The incident beam was initially collimated and subsequently directed through an aperture to reduce the size, and then entered the MPC at a particular angle. After hundreds of reflections, the beam would exit from the other side, two wedge-shaped mirrors were used as the optical windows so that no optical interference occurs. The beam subsequently hit the QTFs by means of a focusing lens. The focal length of the lens is 10 mm and the maximum signal was generated when laser hits the root of a QTF, and the target points on QTFs are shown in Fig. 3.

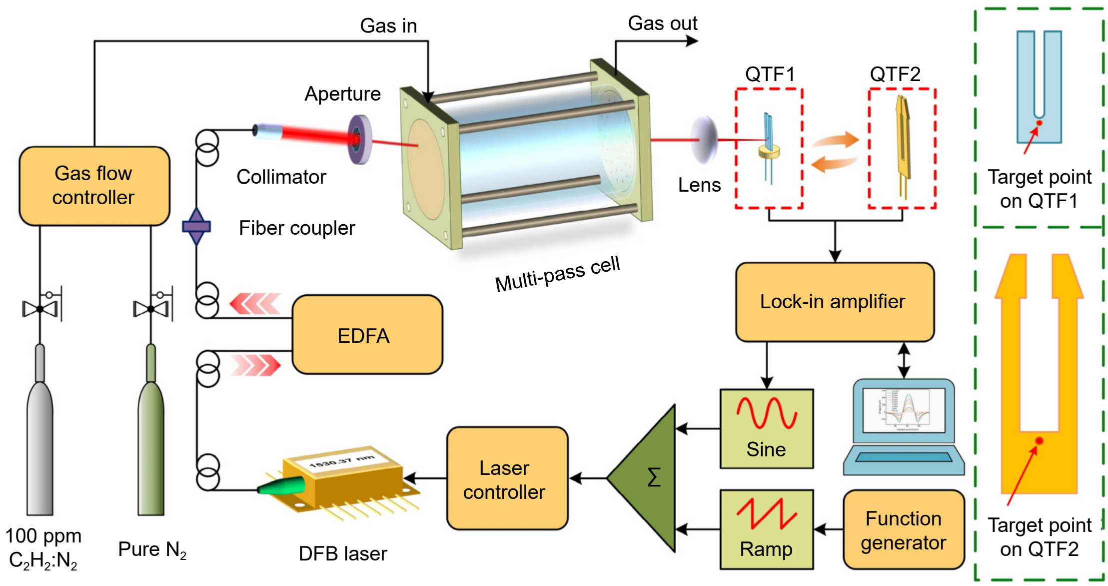

Fig. 3 | Schematic configuration of LITES sensor based on a multi-pass cell with dense spot pattern.

In order to reduce the background noise, wavelength modulation spectroscopy and the 2nd harmonic demodulation techniques were adopted. A function generator was used to generate a ramp wave with a period of 100 s so that the laser output wavelength was scanned through the target absorption line. The lock-in amplifier generated a sine wave that modulated the laser wavelength and was also used as a reference signal for demodulation. The frequencies of the sine wave were set to half the resonance frequencies of the QTFs. Diode lasers have different wavelength response at different modulation frequencies, which result in different optimal modulation currents. The higher the modulation frequency, the smaller the wavelength response, which means there is a smaller change in wavelength with a unit change of current. Therefore, in order to obtain the same range of wavelength change, a larger modulation current is required at high modulation frequency[63]. Therefore, the systems using QTF1 and QTF2 had different current modulation depths of 27.36 mA and 19.18 mA, respectively. The integration times of the lock-in amplifier were respectively set to 120 ms and 240 ms for those two QTFs, and the detection bandwidths were 577 mHz and 288.5 mHz, respectively.

Results and discussion

Experimental results and discussion

Firstly, 2*f*-LITES signal was measured in 100 ppm C_2H_2:N_2 gas mixture. Figure 4(a) and 4(b) show the variation of the peak values with different output power of EDFA when QTF1 and QTF2 were used as the detectors, respectively, and the insets show the respective 2*f* signal waveform. The peak value of the 2*f*-LITES signal has an excellent linear relationship with the optical output power of EDFA. The noise and signal noise ratio (SNR) at different laser powers are shown in Fig. 4(c), when QTF1 and QTF2 were adopted, respectively. The system using two different QTFs has a similar trend. There is a

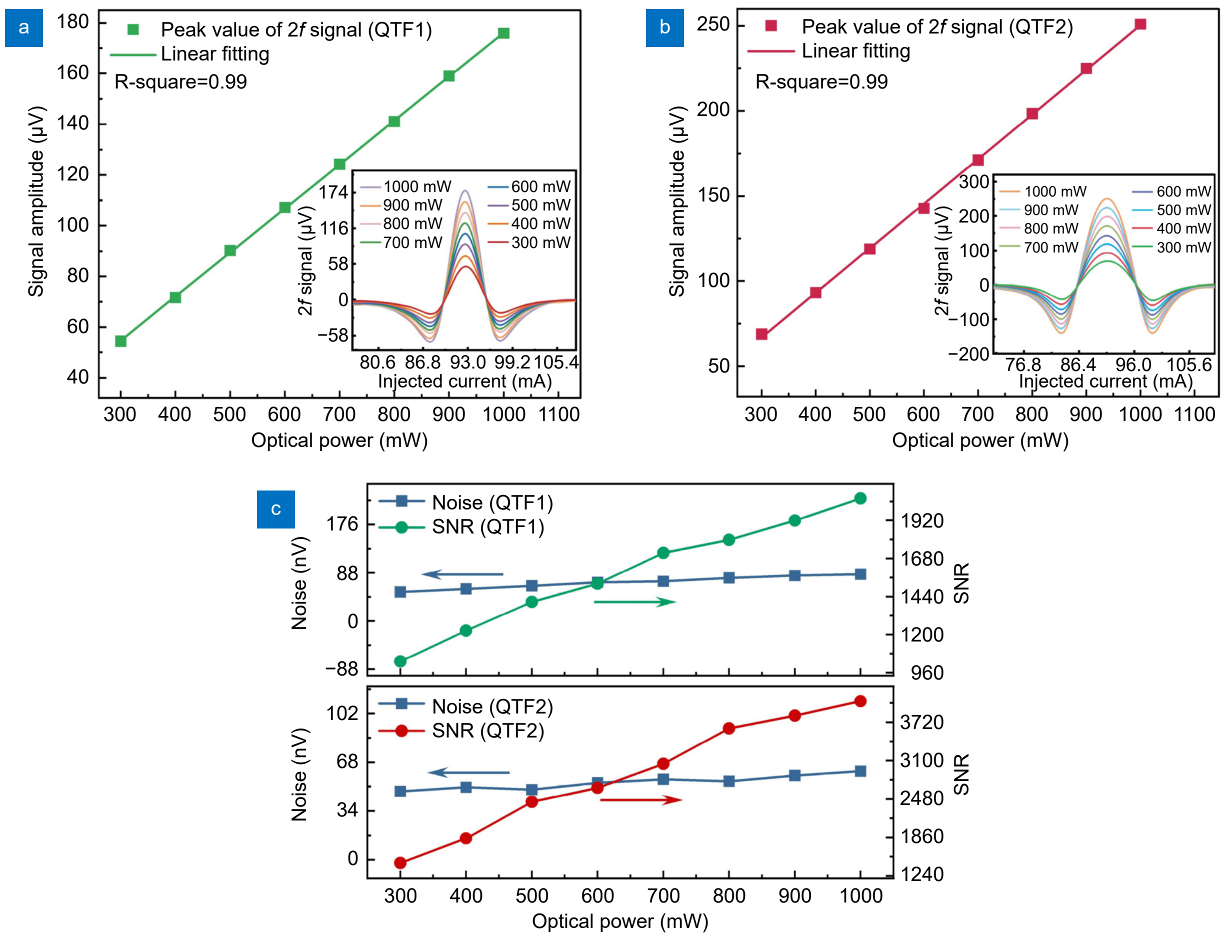

Fig. 4 | System characteristics at different optical powers. (**a**) Peak value of 2*f* signal of the commercial QTF based system. Inset: 2*f* signal waveform. (**b**) Peak value of 2*f* signal of the trapezoidal-tip QTF based system. Inset: 2*f* signal waveform. (**c**) Noise and SNR of the system when commercial QTF and trapezoidal-tip QTF were adopted, respectively.

small increase in noise and a significant increase in SNR as the laser power increased. Therefore, all subsequent experiments were performed with the output power of EDFA at 1000 mW, which produced the highest SNR.

Two gas mass flow meters were used to control the flow rate of a bottle of 100 ppm C_2H_2:N_2 standard gas mixture and a bottle of pure N_2 to obtain different concentrations of C_2H_2. It should be noted that the total flow rate of the gas was kept at 240 mL/min. The 2*f*-LITES signals detected at different concentrations when QTF1 and QTF2 were used as detectors are shown in Fig. 5(a) and 5(b), respectively. At a concentration of 100 ppm, the 2*f* signal peak measured with QTF1 was 176.92 μV, while the value measured with QTF2 was 250.30 μV. The latter is 1.4 times higher than the former, which can be attributed to the lower resonance frequency of the trapezoidal-tip QTF. This character has led to an extended duration for energy accumulation. Figure 5(c) and 5(d) display the peak values of the 2*f* signal at various concentrations, as well as the results after linear fitting. Both exhibit an excellent level of linearity.

The background noise was measured when pure N_2 was used to fill the MPC with a flow rate of 240 mL/min and the output wavelength of the laser was locked at the target absorption line of C_2H_2. The standard deviation (1σ) noise obtained from continuous monitoring of 2*f* amplitude for 60 s and values of 85.50 nV for the system using QTF1 as well as 61.80 nV for the system using QTF2 is shown in Fig. 6. Consequently, the minimum detection limit (MDL) of C_2H_2-LITES sensor using two different QTFs can be calculated from the ratio of the standard gas concentration to the SNR of the corresponding system. The achieved MDL for the C_2H_2-LITES sensor based on QTF1 and QTF2 were 48.3 ppb and 24.6 ppb, respectively. There is an enhancement of the system's detection performance by a factor of 1.96 when replacing the commercial QTF with the self-designed trapezoidal-tip QTF.

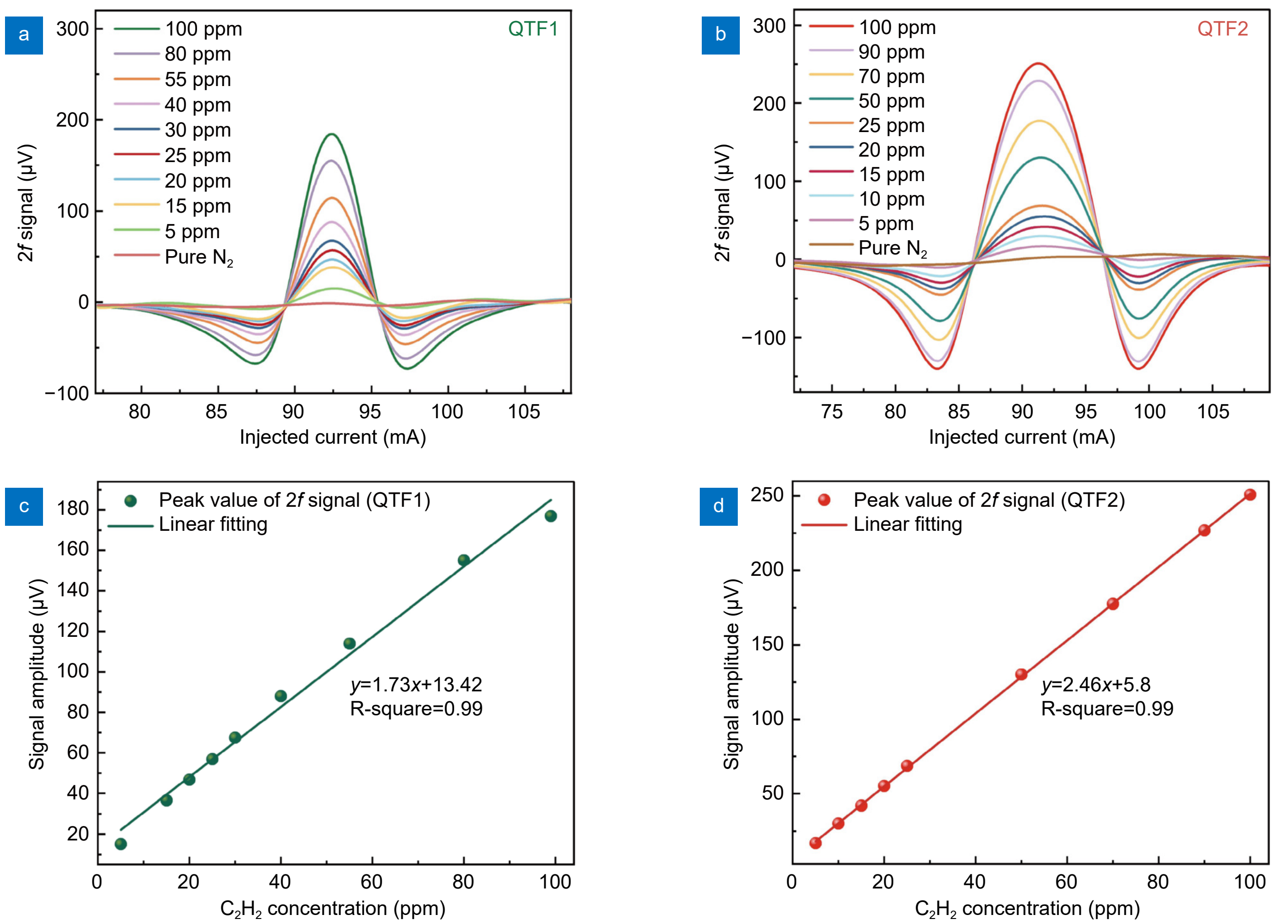

Fig. 5 | (**a**) 2*f* signal at different concentrations when commercial QTF was used. (**b**) 2*f* signal at different concentrations when trapezoidal-tip QTF was used. (**c**)The function relationship between different concentrations and the peak value of the 2*f* signals when commercial QTF was used. (**d**) The function relationship between different concentrations and the peak value of the 2f signals when trapezoidal-tip QTF was used.

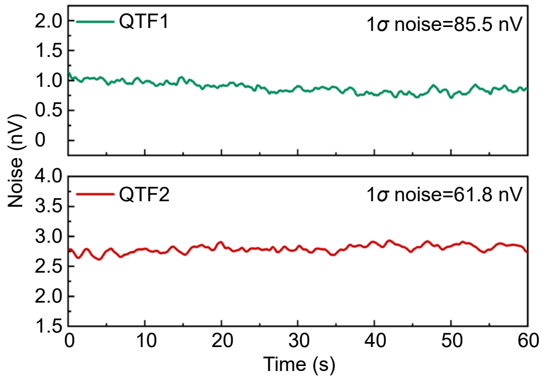

Fig. 6 | Background noise of the LITES sensor system when different QTFs were used as the detector.

The long-term stability of the system can be reflected by the Allan deviations shown in Fig. 7, where Fig. 7(a) shows the results probed with QTF1 and Fig. 7(b) with QTF2. The raw data were obtained by locking the laser output wavelength at the target absorption line and continuously monitoring the 2*f* signal amplitude for more than 2 hours in a pure N_2 atmosphere. The MDL of the QTF1 based C_2H_2-LITES sensor can be improved to 2.61 ppb when the average time is 100 s and the MDL of the QTF2 based system can be enhanced to 1.29 ppb when the average time is 140 s. Due to its large size of QTF, the system using trapezoidal-tipped QTF had better long-term stability.

Conclusion

In conclusion, a highly sensitive LITES sensor based on a MPC with dense spot pattern and a novel QTF with low resonance frequency is reported for the first time. C_2H_2 was selected as the target gas to examine the performance of the system. The MPC has an OPL of 37.7 m and an excellent RLV of 13.8 cm^{-2}. Additionally, a self-designed QTF with trapezoidal-tip and low resonance frequency of 9641.83 Hz was used to improve the detection performance. An EDFA was employed to amplify the output power of the used diode laser to further enhance the signal level. At an optical power of 1000 mW, the MDL of the C_2H_2-LITES sensor based on trapezoidal-tip QTF was determined to be 24.6 ppb, which was 1.96 times better than the system using a commercial QTF with a resonance frequency of 32.753 kHz. Allan deviation analysis showed that the MDL of the commercial QTF based C_2H_2-LITES sensor could be reduced to 2.61 ppb at an average time of 100 s, whereas the system using the trapezoidal-tip QTF could achieve a MDL of 1.29 ppb at an average time of 140 s. The detection performance of this system can be further enhanced by designing MPCs with a larger RLV and better output beam quality. In addition, research on the design of new QTFs with low resonance frequency and high Q-factor can further promote the development of LITES technology. Furthermore, the study of QTF structures that enable multiple excitations will also be effective in enhancing the system performance.

References

1. Wu LM, Yuan XX, Tang YX et al. MXene sensors based on optical and electrical sensing signals: from biological, chemical, and physical sensing to emerging intelligent and bionic devices. *PhotoniX* **4**, 15 (2023).
2. Ma YF, Lewicki R, Razeghi M et al. QEPAS based ppb-level detection of CO and N_2O using a high power CW DFB-QCL. *Opt Express* **21**, 1008–1019 (2013).
3. Yan M, Luo PL, Iwakuni K et al. Mid-infrared dual-comb spectro-

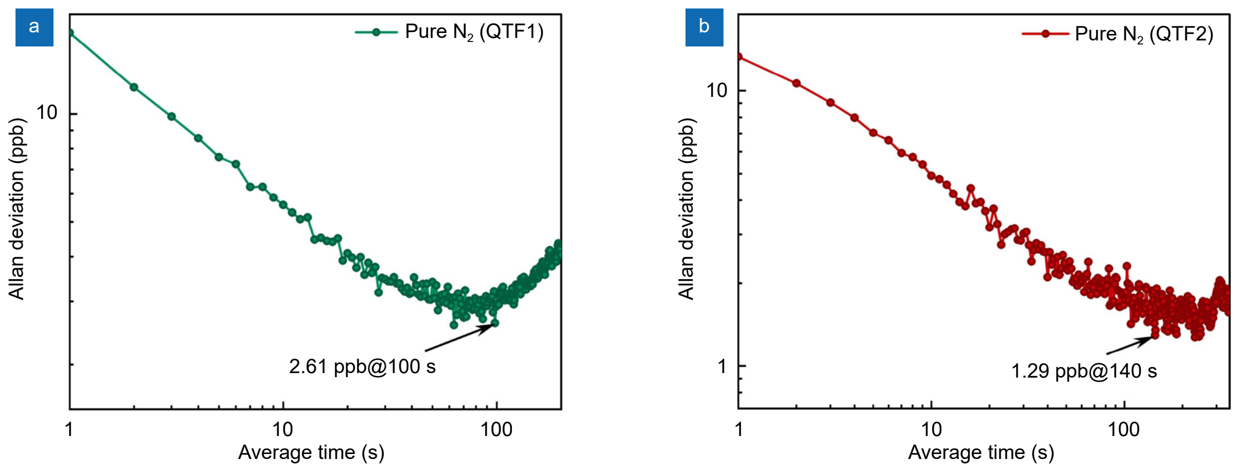

Fig. 7 | Allan deviation analysis. (**a**) Allan deviation analysis for commercial QTF based C_2H_2-LITES sensor. (**b**) Allan deviation analysis for trapezoidal-tip QTF based C_2H_2-LITES sensor.

scopy with electro-optic modulators. *Light Sci Appl* **6**, e17076 (2017).

4. Qi YF, Liu YH, Luo JB. Recent application of Raman spectroscopy in tumor diagnosis: from conventional methods to artificial intelligence fusion. *PhotoniX* **4**, 22 (2023).
5. Zhang C, He Y, Qiao SD et al. Differential integrating sphere-based photoacoustic spectroscopy gas sensing. *Opt Lett* **48**, 5089–5092 (2023).
6. Xu BX, Fan XY, Wang S et al. Sub-femtometer-resolution absolute spectroscopy with sweeping electro-optic combs. *Opto-Electron Adv* **5**, 210023 (2022).
7. Liu XN, Ma YF. New temperature measurement method based on light-induced thermoelastic spectroscopy. *Opt Lett* **48**, 5687–5690 (2023).
8. Leal-Junior A, Avellar L, Biazi V et al. Multifunctional flexible optical waveguide sensor: on the bioinspiration for ultrasensitive sensors development. *Opto-Electron Adv* **5**, 210098 (2022).
9. Chen WP, Qiao SD, Zhao ZX et al. Sensitive carbon monoxide detection based on laser absorption spectroscopy with hollow-core antiresonant fiber. *Microw Opt Technol Lett* **66**, e33780 (2024).
10. Jiang SL, Chen FF, Zhao Y et al. Broadband all-fiber optical phase modulator based on photo-thermal effect in a gas-filled hollow-core fiber. *Opto-Electron Adv* **6**, 220085 (2023).
11. Zhang ZD, Peng T, Nie XY et al. Entangled photons enabled time-frequency-resolved coherent Raman spectroscopy and applications to electronic coherences at femtosecond scale. *Light Sci Appl* **11**, 274 (2022).
12. Li A, Wang C, Bao FX et al. An integrated single-shot spectrometer with large bandwidth-resolution ratio and wide operation temperature range. *PhotoniX* **4**, 29 (2023).
13. Hashimoto K, Nakamura T, Kageyama T et al. Upconversion time-stretch infrared spectroscopy. *Light Sci Appl* **12**, 48 (2023).
14. Lang ZT, Qiao SD, Liang TT et al. Dual-frequency modulated heterodyne quartz-enhanced photoacoustic spectroscopy. *Opt Express* **32**, 379–386 (2024).
15. Yang W, Knorr F, Latka I et al. Real-time molecular imaging of near-surface tissue using Raman spectroscopy. *Light Sci Appl* **11**, 90 (2022).
16. Wang T, Jiang JF, Liu K et al. Flexible minimally invasive coherent anti-Stokes Raman spectroscopy (CARS) measurement method with tapered optical fiber probe for single-cell application. *PhotoniX* **3**, 11 (2022).
17. Le JM, Su YD, Tian CS et al. A novel scheme for ultrashort terahertz pulse generation over a gapless wide spectral range: Raman-resonance-enhanced four-wave mixing. *Light Sci Appl* **12**, 34 (2023).
18. Wang H, Zhan ZY, Hu FT et al. Intelligent optoelectronic processor for orbital angular momentum spectrum measurement. *PhotoniX* **4**, 9 (2023).
19. Yang LY, Li YP, Fang F et al. Highly sensitive and miniature microfiber-based ultrasound sensor for photoacoustic tomography. *Opto-Electron Adv* **5**, 200076 (2022).
20. Vlk M, Datta A, Alberti S et al. Extraordinary evanescent field confinement waveguide sensor for mid-infrared trace gas spectroscopy. *Light Sci Appl* **10**, 26 (2021).
21. Wang YQ, Zhang JH, Zheng YC et al. Brillouin scattering spectrum for liquid detection and applications in oceanography. *Opto-Electron Adv* **6**, 220016 (2023).
22. Chen J, Hangauer A, Strzoda R et al. Laser spectroscopic oxygen sensor using diffuse reflector based optical cell and advanced signal processing. *Appl Phys B* **100**, 417–425 (2010).
23. Chao X, Shen GF, Sun K et al. Cavity-enhanced absorption spectroscopy for shocktubes: design and optimization. *Proc Combust Inst* **37**, 1345–1353 (2019).
24. Zheng KY, Zheng CT, Zhang Y et al. Review of incoherent broadband cavity-enhanced absorption spectroscopy (IBBCEAS) for gas sensing. *Sensors* **18**, 3646 (2018).
25. Zhou XB, Zhao G, Liu JX et al. Fiber pigtailed DFB laser-based optical feedback cavity enhanced absorption spectroscopy with a fiber-coupled EOM for phase correction. *Opt Express* **30**, 6332–6340 (2022).
26. Kosterev AA, Bakhirkin YA, Curl RF et al. Quartz-enhanced photoacoustic spectroscopy. *Opt Lett* **27**, 1902–1904 (2002).
27. Liu K, Mei JX, Zhang WJ et al. Multi-resonator photoacoustic spectroscopy. *Sens Actuators B:Chem* **251**, 632–636 (2017).
28. Zhang C, Qiao SD, He Y et al. Differential quartz-enhanced photoacoustic spectroscopy. *Appl Phys Lett* **122**, 241103 (2023).
29. Wang FP, Xue QS, Chang J et al. Wavelength scanning Q-switched fiber-ring laser intra-cavity QEPAS using a standard 32.76 kHz quartz tuning fork for acetylene detection. *Opt Laser Technol* **134**, 106612 (2021).
30. Wang FP, Cheng YP, Xue QS et al. Techniques to enhance the photoacoustic signal for trace gas sensing: a review. *Sens Actuators A:Phys* **345**, 113807 (2022).
31. Lang ZT, Qiao SD, Ma YF. Acoustic microresonator based in-plane quartz-enhanced photoacoustic spectroscopy sensor with a line interaction mode. *Opt Lett* **47**, 1295–1298 (2022).
32. Rousseau R, Loghmari Z, Bahriz M et al. Off-beam QEPAS sensor using an 11-μm DFB-QCL with an optimized acoustic resonator. *Opt Express* **27**, 7435–7446 (2019).
33. Liu XN, Qiao SD, Han GW et al. Highly sensitive HF detection based on absorption enhanced light-induced thermoelastic spectroscopy with a quartz tuning fork of receive and shallow neural network fitting. *Photoacoustics* **28**, 100422 (2022).
34. Ma YF, He Y, Yu X et al. HCl ppb-level detection based on QEPAS sensor using a low resonance frequency quartz tuning fork. *Sens Actuators B:Chem* **233**, 388–393 (2016).
35. Wu HP, Sampaolo A, Dong L et al. Quartz enhanced photoacoustic H_2S gas sensor based on a fiber-amplifier source and a custom tuning fork with large prong spacing. *Appl Phys Lett* **107**, 111104 (2015).
36. Ma YF, He Y, Tong Y et al. Quartz-tuning-fork enhanced photothermal spectroscopy for ultra-high sensitive trace gas detection. *Opt Express* **26**, 32103–32110 (2018).
37. Chen WP, Qiao SD, Lang ZT et al. Hollow-waveguide-based light-induced thermoelastic spectroscopy sensing. *Opt Lett* **48**, 3989–3992 (2023).
38. Sun B, Patimisco P, Sampaolo A et al. Light-induced thermoelastic sensor for ppb-level H_2S detection in a SF_6 gas matrices exploiting a mini-multi-pass cell and quartz tuning fork photodetector. *Photoacoustics* **33**, 100553 (2023).
39. Liu XN, Ma YF. Sensitive carbon monoxide detection based on light-induced thermoelastic spectroscopy with a fiber-coupled multipass cell [Invited]. *Chin Opt Lett* **20**, 031201 (2022).
40. Hu LE, Zheng CT, Zhang MH et al. Long-distance in-situ methane detection using near-infrared light-induced thermo-elastic spectroscopy. *Photoacoustics* **21**, 100230 (2021).
41. Ma YF, Hu YQ, Qiao SD et al. Quartz tuning forks resonance

frequency matching for laser spectroscopy sensing. *Photoacoustics* **25**, 100329 (2022).
42. Qiao SD, Ma PZ, Tsepelin V et al. Super tiny quartz-tuning-fork-based light-induced thermoelastic spectroscopy sensing. *Opt Lett* **48**, 419–422 (2023).
43. Lang ZT, Qiao SD, Ma YF. Fabry–Perot-based phase demodulation of heterodyne light-induced thermoelastic spectroscopy. *Light Adv Manuf* **4**, 23 (2023).
44. Ma YF, Liang TT, Qiao SD et al. Highly sensitive and fast hydrogen detection based on light-induced thermoelastic spectroscopy. *Ultrafast Sci* **3**, 0024 (2023).
45. Zhao XY, Guo M, Cui DY et al. Multi-pass differential photoacoustic sensor for real-time measurement of SF_6 decomposition component H_2S at the ppb level. *Anal Chem* **95**, 8214–8222 (2023).
46. Liu YH, Ma YF. Advances in multipass cell for absorption spectroscopy- based trace gas sensing technology [Invited]. *Chin Opt Lett* **21**, 033001 (2023).
47. Cao YN, Xu Z, Tian X et al. Generalized calculation model of different types of optical multi-pass cells based on refraction and reflection law. *Opt Laser Technol* **139**, 106958 (2021).
48. He Y, Ma YF, Tong Y et al. Ultra-high sensitive light-induced thermoelastic spectroscopy sensor with a high *Q*-factor quartz tuning fork and a multipass cell. *Opt Lett* **44**, 1904–1907 (2019).
49. Chen HD, Chen C, Wang YZ. Auto-design of multi-pass cell with small size and long optical path length using parallel multi-population genetic algorithm. *IEEE Sens J* **22**, 6518–6527 (2022).
50. Cui RY, Dong L, Wu HP et al. Generalized optical design of two-spherical-mirror multi-pass cells with dense multi-circle spot patterns. *Appl Phys Lett* **116**, 091103 (2020).
51. Hudzikowski A, Głuszek A, Krzempek K et al. Compact, spherical mirror-based dense astigmatic-like pattern multipass cell design aided by a genetic algorithm. *Opt Express* **29**, 26127–26136 (2021).
52. Wei TT, Wu HP, Dong L et al. Palm-sized methane TDLAS sensor based on a mini-multi-pass cell and a quartz tuning fork as a thermal detector. *Opt Express* **29**, 12357–12364 (2021).
53. Zhang C, Qiao SD, Ma YF. Highly sensitive photoacoustic acetylene detection based on differential photoacoustic cell with retro-reflection-cavity. *Photoacoustics* **30**, 100467 (2023).
54. Fang C, Qiao SD, He Y et al. Design and sensing performance of T-shaped quartz tuning forks. *Acta Opt Sin* **43**, 1899910 (2023).
55. Lou CG, Dai JL, Wang YX et al. Highly sensitive light-induced thermoelastic spectroscopy oxygen sensor with co-coupling photoelectric and thermoelastic effect of quartz tuning fork. *Photoacoustics* **31**, 100515 (2023).
56. Lin HY, Zheng HD, Montano BAZ et al. Ppb-level gas detection using on-beam quartz-enhanced photoacoustic spectroscopy based on a 28 kHz tuning fork. *Photoacoustics* **25**, 100321 (2022).
57. Bernstein HJ, Herzberg G. Rotation-vibration spectra of diatomic and simple polyatomic molecules with long absorbing paths. I. The spectrum of Fluoroform (CHF_3) from 2.4μ to 0.7μ. *J Chem Phys* **16**, 30–39 (1948).
58. Herriott DR, Schulte HJ. Folded optical delay lines. *Appl Opt* **4**, 883–889 (1965).
59. Herriott D, Kogelnik H, Kompfner R. Off-axis paths in spherical mirror interferometers. *Appl Opt* **3**, 523–526 (1964).
60. Cui RY, Dong L, Wu HP et al. Calculation model of dense spot pattern multi-pass cells based on a spherical mirror aberration. *Opt Lett* **44**, 1108–1111 (2019).
61. Liu JH, Chen YZ, Xu L et al. Generalized optical design and optimization of multipass cells with independent circle patterns based on the Monte Carlo and Nelder-Mead simplex algorithms. *Opt Express* **29**, 20250–20261 (2021).
62. Patimisco P, Sampaolo A, Dong L et al. Analysis of the electro-elastic properties of custom quartz tuning forks for optoacoustic gas sensing. *Sens Actuators B:Chem* **227**, 539–546 (2016).
63. Sun JC, Chang J, Wang FP et al. Tuning efficiency of distributed feedback laser diode for wavelength modulation spectroscopy. *IEEE Sens J* **19**, 9722–9727 (2019).

Acknowledgements

National Natural Science Foundation of China (Grant Nos. 62335006, 62022032, 62275065, and 61875047), Key Laboratory of Opto-Electronic Information Acquisition and Manipulation (Anhui University), Ministry of Education (Grant No. OEIAM202202), Fundamental Research Funds for the Central Universities (Grant No. HIT.OCEF.2023011).

Author contributions

Y. F. Ma proposed the original idea and supervised the whole project. Y. H. Liu performed the measurements. S. D. Qiao, C. Fang and H. Y. Sun involved in the investigations. Y. He and J. Liu contributed to the discussion and the revision of manuscript.

Competing interests

The authors declare no competing financial interests.

Scan for Article PDF